

Avoided-crossing spectroscopy technique based on detection of atoms in metastable statesA. Mihelič,^{1,*} M. Žitnik,^{1,2} K. Bučar,¹ L. Avaldi,³ and R. Richter⁴¹*Jožef Stefan Institute, Jamova cesta 39, SI-1000 Ljubljana, Slovenia*²*Faculty of Mathematics and Physics, Jadranska ulica 19, SI-1000 Ljubljana, Slovenia*³*CNR-IMIP, Area della Ricerca di Roma 1, Monterotondo Scalo, Rome, Italy*⁴*Sincrotrone Trieste, AREA Science Park, I-34149 Basovizza (Trieste), Italy*

(Received 24 December 2013; revised manuscript received 27 April 2014; published 30 June 2014)

We present a highly efficient technique for observing an avoided-crossing signal resulting from modified decay branching ratios of excited atomic states in the vicinity of avoided crossings (ACs) formed in tunable external fields. The technique is based on detection of atoms in metastable (MS) states, and we apply it to the case of photoexcited helium atoms which cascade to the singlet and triplet $1s2s$ states in a dc electric field. We show that narrow structures present in the MS atom yield are due to the increased probability to cascade to the triplet MS states at the field strengths at which the ACs emerge. The resolution of the present technique is not limited by the excitation bandwidth, only by the extent to which a homogeneous field can be produced over a limited region of space. Using results of high-precision calculations which include relativistic and QED corrections, we are able to reproduce the dependence of the measured MS atom yield on the electric-field strength.

DOI: [10.1103/PhysRevA.89.063422](https://doi.org/10.1103/PhysRevA.89.063422)

PACS number(s): 32.60.+i, 32.80.-t, 32.10.Fn

I. INTRODUCTION

In avoided-crossing spectroscopy, a change in a measured signal is observed which is a consequence of tunable interactions between quantum-mechanical states in those regions of the coupling parameter (e.g., the strength of an external field) where avoided crossings (ACs) emerge. AC spectroscopy techniques are used to study the properties of excited atomic states which are coupled through externally induced interactions, usually with tunable electric or magnetic fields. One of the advantages of using external fields is that the properties of optically forbidden states can be studied [1]. During the past decades, these techniques were frequently used to study fine and hyperfine interactions of excited atomic species [2–8] and also in molecular-beam [9] and solid-state spectroscopy [10]. Compared to conventional spectroscopy, where the energy levels are directly observable, AC techniques may also be successfully applied when the level separation is below the excitation (laser) bandwidth. For example, in a method proposed by Stoneman *et al.* [7,8], a combination of a laser and 300 K blackbody radiation was used to study ACs of the potassium Rydberg p and s states in a dc electric field. On the detection side, the fluorescence signal may be measured to observe the character of the states or their modification when the field strength is tuned across the ACs. A recent example of the former is the hitherto disregarded radiative decay of the He doubly excited states below the second ionization threshold. Using an apparatus in which vacuum ultraviolet photons and atoms in the metastable (MS) states populated in radiative cascades were detected [11], excitations to LS -forbidden doubly excited states could be observed [12,13]. Recently, the singlet-triplet (S-T) mixing in He was studied by recording the triplet metastable atom yield resulting from radiative decay of doubly excited states using a singlet-quenching discharge lamp [14]. A question arose about the influence of the spin-forbidden transitions between

the $1sn\ell$ states on the triplet metastable atom yield since, for angular momentum $\ell \geq 3$, the 1L_L - 3L_L mixing is almost complete [15]. This stimulated studies of the combined effect of the Stark and S-T mixing on the spectra of emitted photons of singly excited helium [16] and the present study.

Here we propose an avoided-crossing technique based on broadband excitation combined with detection of atoms in metastable states. The technique also presents an opportunity to test the results of the high-precision calculations of Drake and collaborators (see Ref. [15] and the references therein) in a complete way.

II. EXPERIMENT

The measurements were performed at the Gas Phase Photoemission beamline of the Elettra synchrotron radiation facility. Linearly polarized synchrotron light (polarization \hat{e}_0) passed through a pair of parallel metal plates separated by 1 cm. A potential difference of up to 12 kV produced an electric field $\mathbf{F} \parallel \hat{e}_0$ [Fig. 1(a)]. The synchrotron beam intersected with a supersonic beam of ground-state He atoms with typical velocities of the order of 1.5 km/s along the beam direction. The dimension of the field plates along the supersonic beam was approximately 3 cm. The slits limiting the photon energy spread were adjusted so that the incident photon energy distribution \mathcal{T} was broad (25–70 meV) and box shaped [a typical measured profile is shown in Fig. 1(b)]. The width of the distribution was chosen to cover the entire energy region of transitions to the field-modified $1sn_1\ell$ states (which will be referred to as the n_1 manifold) but was still narrow enough that no transitions to the states of the adjacent manifolds were induced. The field strengths were low enough that the intermanifold coupling remained negligible for $n_1 \leq 10$. In this way we were able to eliminate the dependence of the excitation probability on the beam profile.

An excited state $|\mu_1\rangle$ of the n_1 manifold decays in the external field via radiative cascades $|\mu_1\rangle \rightarrow |\mu_2\rangle \rightarrow \dots$, which end either in the ground state $|g\rangle$ or one of the $1s2s$ states $|f\rangle$ [Fig. 1(b)]. The total metastable atom yield (MY)

*andrej.mihelic@ijs.si

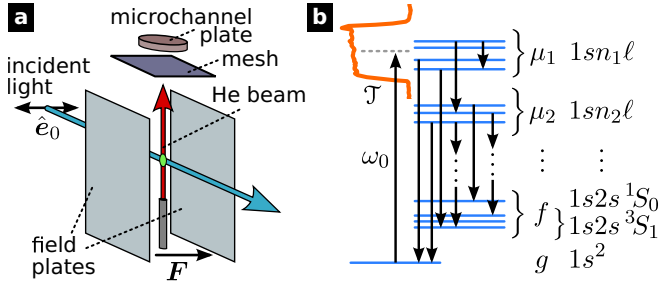


FIG. 1. (Color online) (a) Experimental setup: \hat{e}_0 , polarization of the incident light; F , electric field. (b) Emission cascade of the photoexcited He atom in a dc electric field (g , ground state; μ_i , excited states; f , final metastable states; T , incident photon energy distribution).

was measured by a metastable atom detector which consists of a microchannel plate (MCP) and a mesh [12–14] and was placed about 50 cm from the field plates. The $F = 0$ lifetime of the singlet (triplet) MS state(s) is $\tau_0 \approx 20$ ms (8000 s) [17,18]. To the lowest order, the $1s2s^1S_0$ lifetime is given by $1/\tau \approx 1/\tau_0 + F^2/(0.84 \text{ s kV}^2/\text{cm}^2)$ because of the $1s2s-1s2p$ mixing, whereas the 3S_1 lifetimes remain unchanged if the weak S-T mixing of the $1s2p$ states is neglected. For the field strengths considered, the premature decay of the MS states is thus improbable since the time of flight through the interaction region is of the order of $20 \mu\text{s}$ and the time needed to reach the MCP is about 0.3 ms. The MS states are therefore treated as stable.

III. ANALYSIS OF THE MEASURED METASTABLE ATOM YIELD

At the end of a decay cascade, the number of atoms in the MS states (f) is described by

$$N = \sum_f \sum_{n=1}^{\infty} \sum_{\mu_1, \dots, \mu_n} \frac{\Gamma_{f, \mu_n}}{\Gamma_{\mu_n}} \left(\prod_{j=1}^{n-1} \frac{\Gamma_{\mu_{j+1}, \mu_j}}{\Gamma_{\mu_j}} \right) N_{\mu_1}^0, \quad (1)$$

where n stands for the number of emission steps. The summation μ_1, \dots, μ_n runs over all the accessible states except the MS states and the ground state. The partial and the total decay widths are denoted by $\Gamma_{\zeta, \beta}$ and Γ_{β} , respectively, and $N_{\mu_1}^0$ denotes the number of atoms in state $|\mu_1\rangle$ after photoexcitation from the ground state. As will be discussed further, the interference due to the overlap between the neighboring $|\mu_1\rangle$ states is negligible because of narrow widths Γ_{μ_1} . Since the energy distribution \mathcal{T} , centered at photon energy ω_0 , is much broader than the widths Γ_{μ_1} , the number of atoms in state $|\mu_1\rangle$ reached from the ground state $|g\rangle$ may be approximated by $N_{\mu_1}^0 \propto |\langle \mu_1 | D(\hat{e}_0) | g \rangle|^2 \mathcal{T}(E_g + \omega_0 - E_{\mu_1})$, where E_g and E_{μ_1} are the energies of the two states and D is the dipole operator. The metastable atom yields reported here are normalized so that the total number of excited atoms is equal to unity:

$$\sum_{\mu_1} N_{\mu_1}^0 = 1. \quad (2)$$

The details of the calculations have been described in Ref. [16]. Briefly, the nonrelativistic atomic Hamiltonian H_0 is diagonalized in the basis of LSJ -coupled basis functions. The

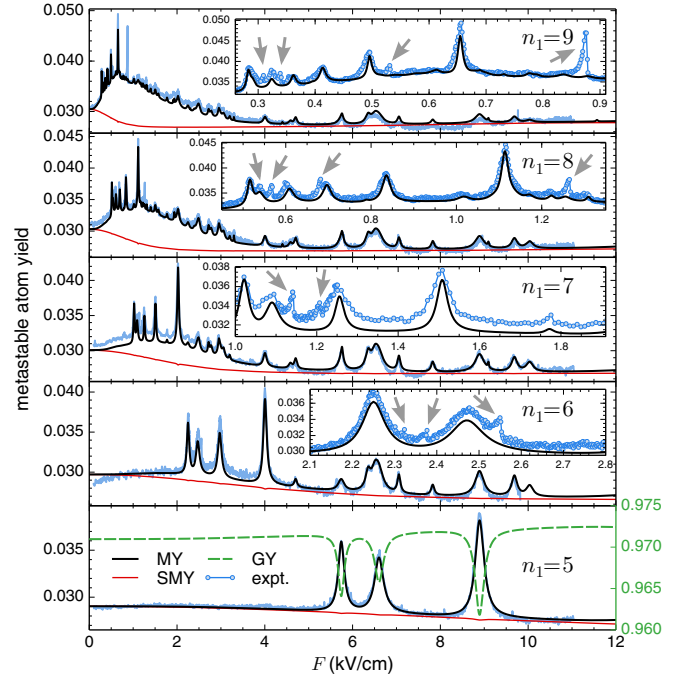


FIG. 2. (Color online) The measured and the calculated total metastable atom yield (MY) for photoexcitation to the n_1 manifolds ($5 \leq n_1 \leq 9$) in a static electric field F . The calculated singlet metastable atom yield (SMY) is plotted with thin red lines, and the dashed green line ($n_1 = 5$ only, right scale) is used for the ground-state yield (GY). The insets show the magnified low- F parts of the plots. The arrows mark the peaks missing in the calculated MY (see text).

eigenfunctions of H_0 are used in the calculation of the atom-field interaction and transition matrix elements. The effect of the external field is taken into account by diagonalizing the total Hamiltonian $H = H_0 + FV = H_0 + F(z_1 + z_2)$ in the basis of the zero-field S-T mixed states, for which the exact energies (with relativistic and QED corrections) and the S-T mixing coefficients are taken from Ref. [15]. We have chosen the direction of the quantization (z) axis along F , so that the projection M of the total angular momentum remains a good quantum number in the external field.

The calculated and the measured dependence of the MY on F are shown in Fig. 2. The vertical scales of the measured MY have been adjusted to match the calculated MY. Furthermore, the experimental field strength has been multiplied by a common scaling factor of 0.92 to bring the positions of the measured peaks into agreement with the theory. This factor is attributed mostly to the field penetration effects [16,19]. An interesting property of the yields is peaked structures which, as our calculations show, are associated with the regions of F where avoided crossings are formed (see Fig. 4). Close to the F values for which the energies of a pair of interacting states lie close to each other (i.e., close to the “center” of the AC), the field-induced mixing between these two states becomes dominant. Since the two states generally cascade to the MS states with different decay probabilities, this results in a change of the MY in this region of F . According to our calculations, the peaks which appear in the total MY are due to the increased triplet MY, whereas the singlet MY remains almost unaffected also at positions where the peaks occur in

the total MY (Fig. 2). The main reason for this is that in the decay of the states of the n_1 manifold, the ground state and the singlet MS state are reached through the singlet $1snp$ basis states, with respective branching ratios of $\sim 97\%$ and $\sim 3\%$ [20]. Due to these strongly asymmetric branching ratios, decay paths which end in the triplet MS states gain most of their intensity from the paths originally leading to the ground state, as can be inferred from the $n_1 = 5$ plot shown in Fig. 2.

A. Behavior close to an avoided crossing

In the following, we outline the theoretical background for the analysis of the measured metastable atom yield. Our treatment is similar to the ones of Refs. [2,8]. Details about the shape of the AC signal can be found in these references. The Hamiltonian operator of the atom in an external dc electric field F may be written as

$$H(F) = H_0 + F V, \quad (3)$$

where H_0 is the Hamiltonian operator of the atom and V describes the atom-field interaction. The quantization (z) axis is assumed to point along F . Let F_c denote the field strength at the center of the selected AC and let $|n\rangle$ and E_n be the eigenstates and the eigenenergies of $H(F_c)$. We may write $H(F)$ in the following way:

$$H(F) = H(F_c) + V \delta F, \quad (4)$$

where we have defined $\delta F = F - F_c$. We assume that the AC is formed due to a strong interaction between a pair of states close to $\delta F = 0$, resulting in the eigenstates of $H(F_c)$ $|a\rangle$ and $|b\rangle$ (Fig. 3). Keeping the terms up to the lowest order in δF , the behavior close to $\delta F = 0$ is described by the following matrix:

$$H = \begin{pmatrix} E_a + \mu_{aa} \delta F^2 & v \delta F \\ v^* \delta F & E_b + \mu_{bb} \delta F^2 \end{pmatrix}, \quad (5)$$

where $v = \langle a|V|b\rangle$ and μ_{aa} and μ_{bb} describe the energy shift due to the coupling of $|a\rangle$ and $|b\rangle$ to the states $\{|n\rangle; n \neq a, b\}$. If we shift the energy origin by $\{-(E_a + E_b - (\mu_{aa} + \mu_{bb}) \delta F^2)/2\}$ and define the energy difference $\delta\epsilon = E_a - E_b + (\mu_{aa} - \mu_{bb}) \delta F^2$, we arrive at

$$H' \approx \begin{pmatrix} -\delta\epsilon/2 & v \delta F \\ v^* \delta F & \delta\epsilon/2 \end{pmatrix} = H'_0 + \delta F V'. \quad (6)$$

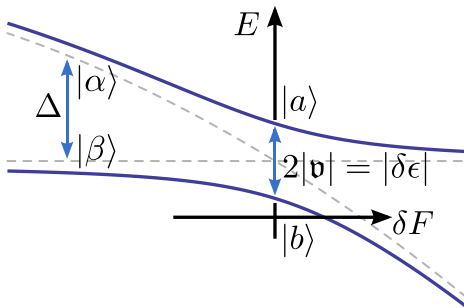


FIG. 3. (Color online) Energy levels as functions of the electric-field strength δF . The dashed lines represent the energy levels in the absence of the coupling v .

Near $\delta F = 0$, the quadratic term $(\mu_{aa} - \mu_{bb}) \delta F^2$ is negligible, and $\delta\epsilon$ may be treated as approximately constant. In this case, $\delta\epsilon \approx \delta\epsilon(\delta F = 0)$ is equal to the minimum energy level splitting, i.e., to the minimum separation between the two energy levels in the Stark diagram. To be able to describe the behavior close to the center of the AC in the basis of the eigenstates of H' for large δF (denoted by $|\alpha\rangle$ and $|\beta\rangle$ in Fig. 3), we transform H' with a unitary transformation of the form

$$U = \begin{pmatrix} \cos \theta & -\sin \theta e^{-i\delta} \\ \sin \theta e^{i\delta} & \cos \theta \end{pmatrix}, \quad (7)$$

where we set $\theta = \pi/4$ and $e^{-i\delta} = v/|v|$. If v is real, U describes a rotation by $\pm\pi/4$. The transformed Hamiltonian matrix is written as

$$H'' = U^\dagger H' U = \begin{pmatrix} -\Delta/2 & v \\ v^* & \Delta/2 \end{pmatrix}, \quad (8)$$

where the off-diagonal matrix element

$$v = \frac{v}{|v|} \frac{\delta\epsilon}{2} \quad (9)$$

describes the (static) coupling between the eigenstates of the atom in the external field far away from $\delta F = 0$ and $\Delta = 2|v| \delta F$ is the difference between the energy levels in the absence of the coupling v (dashed lines in Fig. 3). The diagonal matrix elements of H'' describe how the energies of the states change if the coupling v is zero. At the center ($\Delta = 0$), the eigenstates of H'' are completely mixed and are represented as 50%:50% mixtures of its basis states. The parametrization of Eq. (8) was also used in Refs. [2,8]. Note that v can be unambiguously associated with the interaction between the unperturbed (zero-field) states, such as the fine or hyperfine interaction, when states $|\alpha\rangle$ and $|\beta\rangle$ are not strongly perturbed by the admixture of other states due to the external field.

The eigenvalues of H' (H'') are

$$E_{1,2} = \mp |v| \sqrt{\delta F^2 + \gamma^2/4} \quad (10)$$

$$= \mp \frac{1}{2} \sqrt{\Delta^2 + 4|v|^2}, \quad (11)$$

where

$$\gamma = |\delta\epsilon/v| = |2v/v|. \quad (12)$$

At the center of the AC, the energy splitting is equal to $|\delta\epsilon| = 2|v|$. Avoided crossings may be conveniently located in the calculated Stark maps by calculating the derivatives

$$\frac{\partial E_j}{\partial(\delta F)} = (-1)^j |v| \delta F / \sqrt{\delta F^2 + \gamma^2/4} = \mathbf{x}_j^\dagger V' \mathbf{x}_j, \quad (13)$$

where $j = 1, 2$ denotes the two eigenenergies and $\mathbf{x}_{1,2}$ are the eigen column vectors of H' . When the electric field is tuned across the region of the AC, the two derivatives form a pair of complementary step-shaped functions [see Figs. 4(b) and 4(c)]. Parameter γ is a measure of the extent of the interaction region and is thus directly connected to the widths of the resulting peaks in the MY. This procedure can be generalized to a more general case of several interacting states by

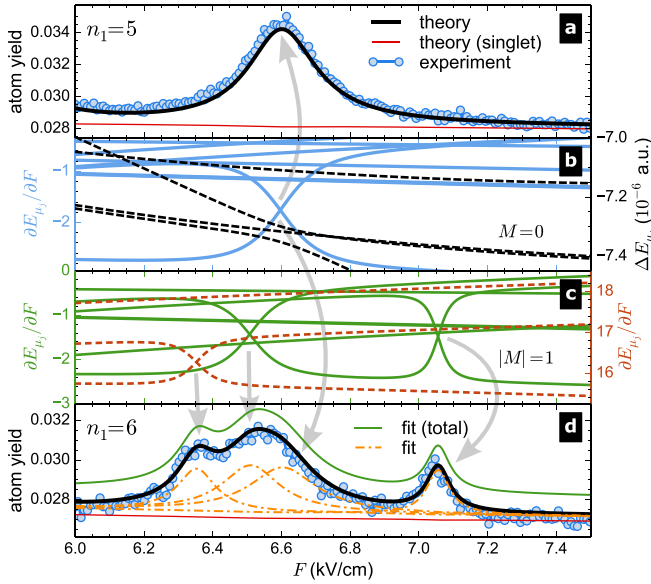


FIG. 4. (Color online) (a) MY for photoexcitation to the $n_1 = 5$ manifold. (b) The calculated eigenenergies (dashed lines, right scale) and the corresponding derivatives for the $n = 5, M = 0$ states ($\Delta E_{\mu_j} = E_{\mu_j} + 2.020$ a.u.). The center of the avoided crossing is at the intersection of the step-shaped curves and coincides with the position of the peak in (a). (c) The derivatives for the $|M| = 1$ states. Two different regions are shown (dashed lines, right scale; solid lines, left scale). (d) MY for $n_1 = 6$. The least-squares fit of the MY with Lorentzian curves is shifted vertically. Contributions of individual peaks are also shown (dash-dotted lines).

replacing the derivative with $\partial E_{\mu_j} / \partial F = \langle \mu_j(F) | V | \mu_j(F) \rangle$. Depending on the branching ratios for the transitions leading to the selected pair of states and on the branching ratios in subsequent steps, one of the possible shapes of the MY may be shown to be Lorentzian $\propto 1/(\delta F^2 + \gamma^2/4)$ [2,8]. Lorentzian peaks are observed also in our case [see Fig. 4(d)]. Note that, in general, other shapes are also possible, e.g., the dispersion-type signal [2,4,8] or the signal resulting from the coherence in excitation and/or decay [21]. It is important to note that in the calculations presented here, Eq. (1) in particular, excitation and decay are treated in an incoherent way. The role of interference effects is discussed below.

The width γ and the field strength F_c can be directly measured with the present experimental setup. Consequently, $|\nu|$ can be calculated from γ [Eq. (12)] if the local field dependence of the energies on the field strength (i.e., the energy difference Δ) is known close to the center of the AC.

B. Discussion

The peaks which appear at higher field strengths in Fig. 2 are due to interactions between the states from lower- n manifolds. Conversely, the peaks which appear at lower field strengths can be associated with the manifolds with higher n . The main reason for this is that the characteristic separation between the energy levels of a selected manifold decreases with increasing n : the larger the typical energy separation is, the higher the field strengths required to strongly couple the states are. Specific

regions of F may thus be directly associated with the principal quantum numbers of the states whose energy levels form ACs. This is also confirmed by the fact that if a peak is present in the MY for a chosen n_1 , peaks also appear in the yields of higher n_1 manifolds at the same value of F .

Exact positions of the peaks in the MY, as well as their widths, depend on the zero-field energies and the dipole interaction matrix elements, which in turn depend on the accurate S-T mixing coefficients. The latter are a crucial ingredient of the present analysis. The measured MY thus represents a strict test of the high-precision calculations of Drake [15].

The number of different cascade paths rapidly increases with the number of steps n . That is why the cascades with higher n contribute non-negligibly to the MY despite their small individual contributions. For $n_1 = 5$, the paths with $n \leq 3$ account only for about 75% of the amplitude of the peak from Fig. 4(a), while for $n \leq 4$, the final spectral shape is roughly reproduced. Although many decay paths generally constitute each peak in the MY, a selected peak may often be associated with a particular pair of energy levels. For $n_1 = 5$, the peak shown in Fig. 4(a) is due to a specific AC: the most probable decay paths for the field strengths around the peak's central position all unambiguously proceed through one of the two $M = 0$ states which form this AC. No other AC is present in this field strength region. A peak centered at the same field strength is present also in the $n_1 = 6$ MY [Fig. 4(d)] but is accompanied by peaks due to ACs among the states with $M = \pm 1$ [Fig. 4(c)]. A change in M is due to an additional step ($n_1 \rightarrow n_2$) needed to reach the MS states through the states of the $n_2 = 5$ manifold. In this sense, the present technique differs from the more established AC techniques in that the signals of all accessible ACs are visible in the specified region of F .

A detailed inspection of the low- F parts of the MY (Fig. 2) reveals that peaks are present in the measured MY which are not reproduced by the calculations. In order to explain these discrepancies, we have examined the effect of electric quadrupole ($E2$) and magnetic dipole ($M1$) decays and the effect of a possible (slight) misalignment of \hat{e}_0 and \mathbf{F} during the experiment. While the $E2$ and $M1$ transitions are too weak to measurably change the yield, a misalignment of \hat{e}_0 and \mathbf{F} by as much as 10° results in additional structures which are either too small or appear at field strengths which do not coincide with the positions of the missing peaks. We have also checked the interference effects by treating photoabsorption and emission of the first photon coherently (i.e., by calculating the inelastic photon-scattering transition amplitudes). The MY calculated in this way is indistinguishable from the yield obtained with the incoherent treatment outlined in the previous section, which is connected to the narrow decay widths of states $|\mu_1\rangle$. Another concern regards the He atoms which leave the interaction region in higher-lying excited states, i.e., the atoms which leave the interaction region before cascading to the ground state or to the MS states. Radiative decay which takes place in the zero-field region, after the atoms leave the interaction region and before they hit the MCP [see Fig. 1(a)], is unlikely to produce additional peaked structures. On the other hand, only ground-state atoms can be distinguished from atoms in excited states with the MCP; the present setup

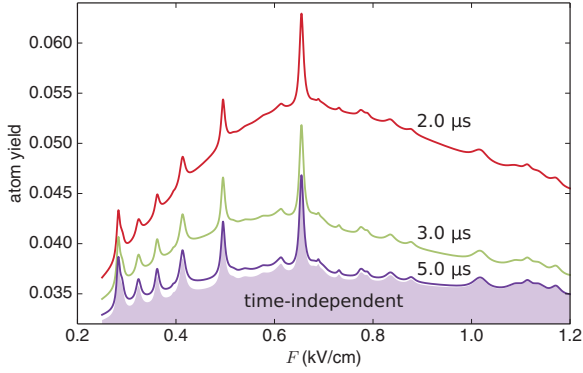


FIG. 5. (Color online) The yield of excited atoms N_e (see text) for $n_1 = 9$ calculated at times 2.0, 3.0, and 5.0 μs after photoexcitation. The shaded plot (bottom) is obtained with the time-independent approach.

does not allow us to differentiate between atoms in the MS states and atoms in higher-lying states. This could result in an increased signal measured by the MCP due to the incomplete decay. To verify this, we have calculated the time-dependent populations of the excited states N_j by solving kinetic equations:

$$\frac{d}{dt}N_j(t) = -\Gamma_j N_j(t) + \sum_k \Gamma_{k,j} N_k(t), \quad (14)$$

with the initial condition $N_j(0) = N_j^0$ describing the number of atoms in state $|j\rangle$ ($j \neq g$) upon photoexcitation. The total yield of excited atoms at time t_0 after photoexcitation is then calculated as

$$N_e(t_0) = \sum_{j \neq g} N_j(t_0). \quad (15)$$

Figure 5 shows the excited atom yield N_e for various values of t_0 for the case of $n_1 = 9$. For $t_0 = 5 \mu\text{s}$, the time-dependent yield is approximately equal to the yield obtained with the time-independent approach (shaded plot in Fig. 5). In this time, the excited atoms have moved by a few millimeters, and most of them have decayed to the ground state or to the MS states. As has been mentioned, the time needed to pass through the interaction region is of the order of 20 μs , which is long enough for the cascade to complete. Furthermore, most of the peaks are discernible already at lower t_0 . We can thus conclude that the peaks do not result from an incomplete decay and the subsequent misidentification of the excited states for the MS states.

Finally, further simulations have shown that the missing peaks could be attributed to the presence of a weak magnetic field $\mathbf{B} \perp \mathbf{F}$ with the magnitude $B_\perp \sim 4 \text{ G}$ (Fig. 6). Subsequent measurements of the magnetic field showed that such a field could have been present during the measurement since the interaction region was not mu-metal shielded during the data acquisition. No assessment of the magnitude of the total magnetic field $(B_\parallel^2 + B_\perp^2)^{1/2}$ can be made because the parallel component results in substantially narrower peaks, effects of which are not measurable with the present setup for $B_\parallel \lesssim 30 \text{ G}$.

The present technique could also be applied to He doubly excited states. In fact, the zero-field MY has recently been

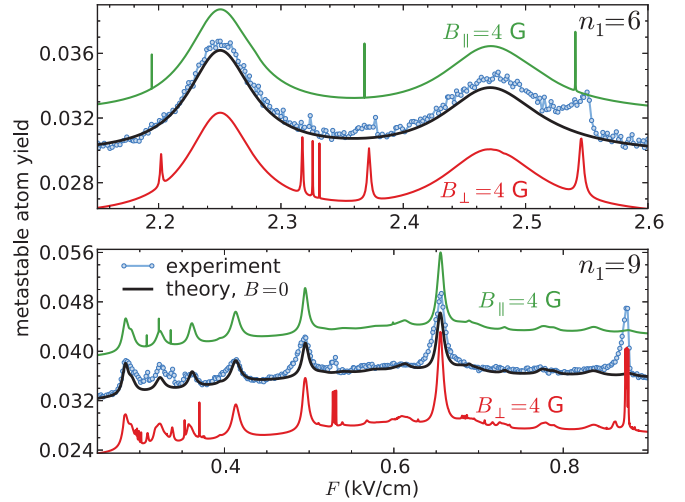


FIG. 6. (Color online) The measured (points) and the calculated metastable atom yield for (top) $n_1 = 6$ and (bottom) $n_1 = 9$. The peaks missing in the theoretical yield (thick black line) appear when a weak magnetic field is included in the calculation.

measured to detect two-photon excitation to the 1^1S^e and 1^1D^e autoionizing states converging to the $N = 2$ ionization threshold [22]. Since these doubly excited states mostly decay to the $1snp$ and $1snf$ states, reliable (zero-field) branching ratios of the $1sn\ell$ states to the metastable states calculated with Eq. (1) turned out to be a crucial ingredient of the analysis.

IV. CONCLUSION

We have presented an avoided-crossing technique based on detection of atoms in metastable states. We have demonstrated its high sensitivity to the field strength variation and its applicability for the case of the helium atom in a dc electric field. Using the present technique, accurate values of the field strength at which avoided crossings are formed can be directly measured. We have shown how the parameters which can be extracted from the field dependence of the metastable atom yield are related to the parameters describing the coupling between the states. The excellent agreement of the calculated metastable atom yield with the measured yield fully validates the accurate state energies and the singlet-triplet mixing coefficients used in the calculation. The sensitivity of the technique is limited only by the ability to control the exact field strengths and to produce a well-defined region of homogeneous field. The present technique can complement traditional spectroscopic techniques and can be extended to doubly excited states, heavier atoms, and other tunable interactions, such as magnetic fields.

ACKNOWLEDGMENTS

A.M., M.Ž., and K.B. acknowledge the financial support of the Ministry of Education, Science and Sport of the Republic of Slovenia (Research Program No. P1-0112). This work was partly supported by the MAE Italy-Slovenia joint project “Dynamics at nanoscale.”

- [1] T. G. Eck, L. L. Foldy, and H. Wieder, *Phys. Rev. Lett.* **10**, 239 (1963).
- [2] H. Wieder and T. G. Eck, *Phys. Rev.* **153**, 103 (1967).
- [3] K. H. Liao, L. K. Lam, R. Gupta, and W. Happer, *Phys. Rev. Lett.* **32**, 1340 (1974).
- [4] T. Andersen, S. Isaksen, D. B. Iversen, and P. S. Ramanujam, *Phys. Rev. A* **18**, 1079 (1978).
- [5] W. M. Itano and I. Ozier, *J. Chem. Phys.* **72**, 3700 (1980).
- [6] R. Panock, R. R. Freeman, B. R. Zegarski, and T. A. Miller, *Phys. Rev. A* **25**, 869 (1982).
- [7] R. C. Stoneman and T. F. Gallagher, *Phys. Rev. Lett.* **55**, 2567 (1985).
- [8] R. C. Stoneman, G. Janik, and T. F. Gallagher, *Phys. Rev. A* **34**, 2952 (1986).
- [9] I. Ozier and W. L. Meerts, *Phys. Rev. Lett.* **40**, 226 (1978).
- [10] A. Wokaun, S. C. Rand, R. G. DeVoe, and R. G. Brewer, *Phys. Rev. B* **23**, 5733 (1981).
- [11] M. K. Odling-Smee, E. Sokell, P. Hammond, and M. A. MacDonald, *Phys. Rev. Lett.* **84**, 2598 (2000).
- [12] F. Penent, P. Lablanquie, R. I. Hall, M. Žitnik, K. Bučar, S. Stranges, R. Richter, M. Alagia, P. Hammond, and J. G. Lambourne, *Phys. Rev. Lett.* **86**, 2758 (2001).
- [13] J. G. Lambourne, F. Penent, P. Lablanquie, R. I. Hall, M. Ahmad, M. Žitnik, K. Bučar, P. Hammond, S. Stranges, R. Richter, M. Alagia, and M. Coreno, *J. Phys. B* **36**, 4339 (2003).
- [14] J.-E. Rubensson, A. Moise, A. Mihelič, K. Bučar, M. Žitnik, and R. Richter, *Phys. Rev. A* **81**, 062510 (2010).
- [15] G. W. F. Drake, in *Handbook of Atomic, Molecular, and Optical Physics*, edited by G. W. F. Drake (Springer, Berlin, 2006), Chap. B11, pp. 199–219.
- [16] A. Mihelič, M. Žitnik, K. C. Prince, M. Coreno, and R. Richter, *Phys. Rev. A* **85**, 023421 (2012).
- [17] R. S. Van Dyck, C. E. Johnson, and H. A. Shugart, *Phys. Rev. A* **4**, 1327 (1971).
- [18] S. S. Hodgman, R. G. Dall, L. J. Byron, K. G. H. Baldwin, S. J. Buckman, and A. G. Truscott, *Phys. Rev. Lett.* **103**, 053002 (2009).
- [19] J. R. Harries, J. P. Sullivan, J. B. Sternberg, S. Obara, T. Suzuki, P. Hammond, J. Bozek, N. Berrah, M. Halka, and Y. Azuma, *Phys. Rev. Lett.* **90**, 133002 (2003).
- [20] M. Žitnik, A. Stanič, K. Bučar, J. G. Lambourne, F. Penent, R. I. Hall, and P. Lablanquie, *J. Phys. B* **36**, 4175 (2003).
- [21] B. Budick and J. Snir, *Phys. Rev. Lett.* **20**, 177 (1968).
- [22] M. Žitnik *et al.* (unpublished).